EPJ manuscript No.
(will be inserted by the editor)

Final-State Interactions in the Process $\vec{p}p \to pK^+\Lambda$

The COSY-TOF Collaboration

M. Röder[a 1,2], E. Borodina[1,2], H. Clement[6,7], E. Doroshkevich[6,7], R. Dzhygadlo[1,2], K. Ehrhardt[6,7], A. Erhardt[6,7], W. Eyrich[5], W. Gast[1,2], A. Gillitzer[1,2], D. Grzonka[1,2], J. Haidenbauer[1,2,3], C. Hanhart[1,2,3], F. Hauenstein[1,2,5], P. Klaja[1,2,5], L. Kober[5], K. Kilian[1,2], M. Krapp[5], M. Mertens[1,2], J. Ritman[1,2], E. Roderburg[1,2], W. Schroeder[2], T. Sefzick[1,2], A. Sibirtsev[8], P. Wintz[1,2], and P. Wüstner[2,4]

[1] Institut für Kernphysik, Forschungszentrum Jülich, 52428 Jülich, Germany
[2] Jülich Center for Hadron Physics, Forschungszentrum Jülich, 52428 Jülich, Germany
[3] Institute for Advanced Simulation, Forschungszentrum Jülich, 52428 Jülich, Germany
[4] Zentralinstitut für Elektronik, Forschungszentrum Jülich, 52428 Jülich, Germany
[5] Friedrich-Alexander-Universität Erlangen-Nürnberg, 91058 Erlangen, Germany
[6] Physikalisches Institut der Universität Tübingen, Auf der Morgenstelle 14, 72076 Tübingen, Germany
[7] Kepler Center for Astro and Particle Physics, University of Tübingen, Auf der Morgenstelle 14, 72076 Tübingen, Germany
[8] Helmholtz-Institut für Strahlen- und Kernphysik, Nussallee 14-16 53115 Bonn, Germany

the date of receipt and acceptance should be inserted later

Abstract. The possibility to determine the $p\Lambda$ scattering length from the final-state interaction in the reaction $\vec{p}p \to pK^+\Lambda$ is investigated experimentally. From a transversely polarized measurement, the K^+ analyzing power (A_N) which, in principle, allows one to extract the spin triplet scattering length is studied. An unexpected energy dependence of the forward/backward symmetric part of A_N is found. The influence of N^* resonances on the $p\Lambda$ invariant mass spectrum is investigated by exploiting the large acceptance for the process $\vec{p}p \to pK^+\Lambda \to pK^+p\pi^-$ and is found to be the main source of uncertainty for determining the $p\Lambda$ scattering length.

PACS. 13.75.-n Hadron-induced low- and intermediate-energy reactions and scattering (energy $\leq$ 10 GeV) – 13.75.Ev Hyperon-nucleon interactions – 25.40.Ve Other reactions above meson production thresholds (energies $>$ 400 MeV)

1 Introduction

While nucleon-nucleon scattering has been precisely measured and accurately described up to beam kinetic energies of 3 GeV [1], the situation is much worse for hyperon-nucleon scattering. Recently, a dispersion relation technique was developed by Gasparyan et al. [2] that allows one to extract the $p\Lambda$ scattering length from final-state interactions in processes with high momentum transfer like $\vec{p}p \to pK^+\Lambda$. It requires data where the $p\Lambda$ system is in a specific total spin (S=0 or S=1). In an experiment with transversely polarized beam, the symmetric component of the K^+ analyzing power (A_N) can be used to disentangle the spin-triplet component of the $p\Lambda$ interaction. Then, the scattering length can be extracted from the shape of the corresponding $p\Lambda$ invariant mass spectrum.

N^* resonances were found to have a significant influence on the $pK\Lambda$ production cross sections [3,4], see also [5]. In Ref. [2] it is pointed out that a Dalitz plot analysis should be performed to check whether the area of $p\Lambda$ final-state interaction is overlapping with those resonance structures in order to assess the applicability of the extraction method.

Due to its unique feature of 4π acceptance for the final state, the COSY-TOF spectrometer is ideally suited to measure the $\vec{p}p \to pK^+\Lambda$ reaction and provide the data needed for the extraction of the scattering length and the Dalitz plot analysis. It has recently been upgraded for improved event reconstruction capabilities. These should allow to achieve an experimental precision that competes with the accuracy of the extraction method. Additionally, the polarized proton beam from the COSY accelerator gives access to the polarization observable A_N.

In this paper we apply the extraction method to data taken at a beam momentum of 2.95 GeV/c, corresponding to an excess energy of 203.7 MeV. Systematic effects due to the influence of N^* resonances are quantified by separately analyzing different regions of the Dalitz plot. We observe an unexpected energy dependence of the K^+ analyzing power, and consequently it is not possible to determine the spin-triplet scattering length at this beam momentum, with the amount of data available. Nevertheless, this finding

[a] m.roeder@fz-juelich.de

is interesting and further experimental and theoretical studies are necessary.

2 Method to Determine the Spin-Triplet Scattering Length (a_t)

The $p\Lambda$ interaction in the final state leads to an enhancement of the production cross section for $p\Lambda$ invariant masses ($m_{p\Lambda}$) near threshold. In Ref. [2] a dispersion relation is derived that connects the $p\Lambda$ scattering length to an integral over $m_{p\Lambda}$. The spectrum is integrated from $m_0 = m_p + m_\Lambda$ up to $m_{\max} = m_0 + 40\,\mathrm{MeV}/c^2$, because the $p\Lambda$ system is required to be in an S-wave. From simulations it is argued that, with this limit, the accuracy of the method is 0.3 fm.

The application of the method requires observables where the $p\Lambda$ system is in a specific total spin state. In Appendix B of Ref. [2] it is pointed out that from a measurement with a transversely polarized beam observables are accessible to which only the spin-triplet part of the production amplitude contributes. Therefore, the spin-triplet scattering length a_t can be determined. To show that, the K^+ analyzing power is expanded in terms of the associated Legendre Polynomials P_ℓ^m of degree ℓ and order m [6]:

$$\begin{aligned} &A_N(\cos\theta_K^*, m_{p\Lambda})\frac{d^2\sigma}{d\cos\theta_K^* dm_{p\Lambda}} \\ &= \alpha(m_{p\Lambda})P_1^1(\cos\theta_K^*) + \beta(m_{p\Lambda})P_2^1(\cos\theta_K^*) + \dots\ . \end{aligned} \tag{1}$$

Here, $d^2\sigma/d\cos\theta_K^* dm_{p\Lambda}$ is the double differential production cross section and θ_K^* is the polar angle of the K^+ in the center-of-mass system. The function P_1^1 (P_2^1) is forward-backward symmetric (antisymmetric). Higher order contributions to Eq. (1) turn out to be negligible in the analysis of the data from the current experiment. This implies that the coefficient α results from the interference of amplitudes that correspond to the K^+ being in an s- and p-wave, respectively, while the coefficient β is due to an interference of the s- and d-wave amplitudes [6].

Under the assumption that the $p\Lambda$ system is in an S-wave, only spin-triplet amplitudes contribute to α (see Appendix B of [2] for details). This follows from the fact that different spin states in the final state do not interfere and that, in addition, for a spin zero $p\Lambda$ final state, only even K^+ partial waves are possible[1]. Consequently, there is no contribution of the $p\Lambda$ singlet state to the K^+ p-wave, hence to α. Therefore, the integral

$$\begin{aligned} &\int_{-1}^{+1} d\cos\theta_K^* \frac{A_N(\cos\theta_K^*, m_{p\Lambda})}{p_{p\Lambda}} \frac{d^2\sigma}{d\cos\theta_K^* dm_{p\Lambda}} \\ &= \alpha(m_{p\Lambda})\frac{\pi}{2}\ , \end{aligned} \tag{2}$$

contains only contributions from $p\Lambda$ spin-triplet states because the forward-backward antisymmetric term proportional to β cancels out. Here, $p_{p\Lambda}$ denotes the relative momentum between p and Λ.

Using the parametrization

$$|\alpha(m_{p\Lambda})| = \exp\left[C_0 + \frac{C_1^2}{(m_{p\Lambda}^2 - C_2^2)}\right], \tag{3}$$

with the free parameters C_i, the spin-triplet scattering length a_t can be obtained from:

$$\begin{aligned} a_t(C_1, C_2) &= -\frac{\hbar c}{2} C_1^2 \\ &\times \sqrt{\left(\frac{m_0^2}{m_p m_\Lambda}\right)\frac{(m_{\max}^2 - m_0^2)}{(m_{\max}^2 - C_2^2)(m_0^2 - C_2^2)^3}}. \end{aligned} \tag{4}$$

The independence of the scattering length from C_0 reflects the fact that only the *shape* induced by the final-state interaction plays a role — this is why already the proportionality of the spin-triplet scattering amplitude to $|\alpha(m_{p\Lambda})|$ alone is sufficient.

Direct measurements of $d\sigma/d\cos\theta_K^*$ have demonstrated that there is practically no dependence of this quantity on θ_K^* [4, 7]. Thus, we can simplify the formalism in the application to the present experiment. Specifically, instead of Eq. (1) we can use

$$\begin{aligned} &A_N(\cos\theta_K^*, m_{p\Lambda}) \\ &= \bar{\alpha}(m_{p\Lambda})P_1^1(\cos\theta_K^*) + \bar{\beta}(m_{p\Lambda})P_2^1(\cos\theta_K^*)\ . \end{aligned} \tag{5}$$

The quantities α and $\bar{\alpha}$ are then simply related by

$$\alpha(m_{p\Lambda}) = \bar{\alpha}(m_{p\Lambda}) \cdot |M(m_{p\Lambda})|^2, \tag{6}$$

where $|M(m_{p\Lambda})|^2$ is proportional to the angular- and spin-averaged enhancement of the production cross section, as discussed above:

$$|M(m_{p\Lambda})|^2 \propto \frac{1}{p_{p\Lambda}}\frac{d\sigma}{dm_{p\Lambda}}. \tag{7}$$

As a consequence we can separately determine the quantities $\bar{\alpha}(m_{p\Lambda})$ and $|M(m_{p\Lambda})|^2$ and then use their product in Eqs. (3-4).

3 Experimental Method

3.1 Experimental Setup

The new experimental setup of COSY-TOF is sketched in Fig. 1. Segmented scintillators close to the target and at the

[1] For a $p\Lambda$ system in an S-wave and in a spin zero state one has for the total angular momentum $J_{\mathrm{tot}} = \ell_K$, with ℓ_K for the angular momentum of the K^+ with respect to the $p\Lambda$ system. The parity of the final state thus reads $\pi_f = (-1)^{\ell_K+1}$. Because the parity of the initial state is given by the relative angular momentum L_i of the protons as $\pi_f = (-1)^{L_i}$, it follows from parity conservation that $L_i \neq J_{\mathrm{tot}}$. Therefore, the initial state can only be in spin 1 state. Because then the Pauli principle demands that $(-1)^{L_i} = -1$, it follows from $L_i \neq \ell_K$ that ℓ_K has to be even.

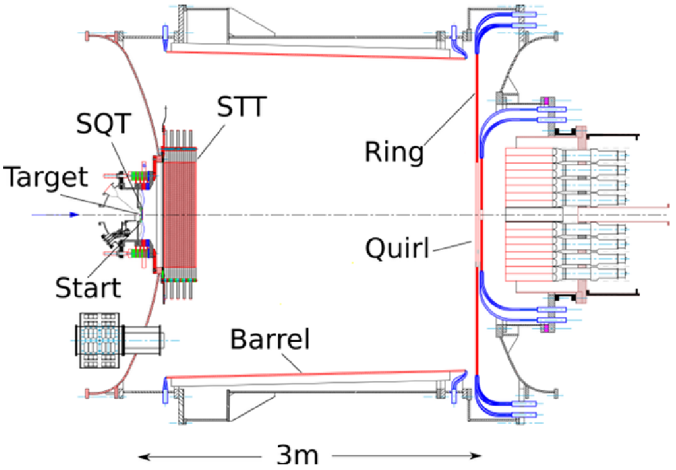

Fig. 1. Schematic view of the COSY-TOF detector, including the new Straw Tube Tracker (STT) and Silicon Quirl Telescope (SQT).

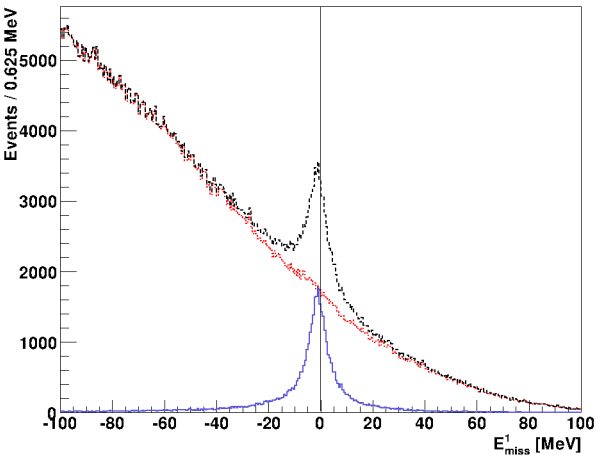

Fig. 2. Missing energy spectrum at the primary vertex. From all events with a successful kinematic fit (dashed line) a sub-sample is selected (blue solid line) as described in the text. Also the complementary sub-sample is shown (red dotted line).

inner side of the main vacuum vessel are used for triggering, time of flight and dE/dx measurements. New detection subsystems have been installed to improve the event reconstruction precision and efficiency: the Silicon Quirl (SQT) close to the target and the Straw Tube Tracker (STT) [8] inside the main vacuum vessel. The STT has nearly 4π acceptance for the $pp \to pK^+\Lambda \to pK^+p\pi$ process and detects all charged particles in the final state, thus it is the most important subsystem for this analysis. It consists of 2704 individual straw tubes combined into 13 double layers normal to the beam axis with 3 azimuthal orientations. The spatial resolution achieved under experimental conditions of the individual straws has been shown to be $\sigma \approx 150\,\mu\text{m}$ with an efficiency better than $\approx 98\%$. For the $pK^+\Lambda$ final state this results in a resolution of $\sigma_m \approx 1.1\,\text{MeV}/c^2$ for the $p\Lambda$ invariant mass at a reconstruction efficiency times acceptance of 25% [7] for the charged decay mode.

3.2 Data Analysis

The primary signature of a good event is the combination of two primary tracks from the target and two tracks from the delayed weak decay of the Λ particle. Additionally, the Λ decay plane contains the primary vertex position. After selecting events that fulfill these criteria, a kinematic fit is performed which minimizes the χ^2_{kin} with respect to the measured track to wire distances in the STT. To reject background processes a threshold is set on the reduced chi-square:

$$\chi^2_{\text{kin}}/\text{NDF} < 5 \ . \tag{8}$$

Additionally, events with a minimum distance s_Λ between the production and decay of the Λ are selected

$$s_\Lambda > 3\,\text{cm} \ . \tag{9}$$

Furthermore, the laboratory angle between the Λ and its decay proton is required to fulfill the condition:

$$\measuredangle(\Lambda, p) > 3\,\text{mrad} \ , \tag{10}$$

in order to reduce instrumental background from events with multiple primary tracks.

The effectiveness of these selection criteria is evaluated by the distribution of the missing energy (E^1_{miss}) at the primary vertex with respect to a $pK^+\Lambda$ final-state hypothesis, before the kinematic fit. This is shown with the dashed line in Fig. 2 for all fit events with $s_\Lambda > 1\,\text{cm}$. The signal peak around 0 MeV lies on top of a continuum from the instrumental background. By applying the criteria in Eqs. (8-10) only events in the peak are selected (solid). At $p_{\text{beam}} = 2.95\,\text{GeV}/c$ a total sample of about 42,000 events is obtained.

Physical background remains from the process $\vec{p}p \to pK^+\Sigma^0 \to pK^+\Lambda\gamma$, where the unmeasured γ carries away $\approx 77\,\text{MeV}$. This results in a deflection of the Λ by $\approx 2^\circ$ in the laboratory frame. The event topologies are therefore similar. Studies of Monte Carlo (MC) generated events have shown that the contamination of the event sample under the conditions in Eqs. (8-10) is $\leq 5\%$. Therefore, it is neglected in the following analysis.

3.3 Determination of the K^+ Analyzing Power A_N

The analyzing power A_N is a measure for the left/right asymmetry ϵ_{LR} of the K^+ differential cross section and is defined as:

$$A_N(\theta^*_K) \equiv \frac{\epsilon_{LR}(\theta^*_K, \phi)}{\cos(\phi) \cdot P} \ . \tag{11}$$

with the beam polarization P. The asymmetry is determined from

$$\epsilon_{LR}(\theta^*_K, \phi) = \frac{L(\theta^*_K, \phi) - R(\theta^*_K, \phi)}{L(\theta^*_K, \phi) + R(\theta^*_K, \phi)} \ , \quad \phi \in \left(-\frac{\pi}{2}, +\frac{\pi}{2}\right) \ , \tag{12}$$

where

$$L(\theta^*_K, \phi) = \sqrt{N^+(\phi) \cdot N^-(\phi + \pi)} \quad \text{and} \quad R(\theta^*_K, \phi) = \sqrt{N^-(\phi) \cdot N^+(\phi + \pi)} \; . \tag{13}$$

Here, $N^{\pm}(\phi)$ is the number of events with spin up (+) and spin down(−) projectiles at the azimuthal angle ϕ. The spin direction was flipped after every extraction cycle (120 s). By multiplying the number of events on the opposite sides of the detector and opposite spin states, systematic effects from asymmetries in the detector acceptance are canceled to first order. The data has been divided into eight bins in the K^+ azimuthal angle ϕ.

The beam polarization was determined with the known analyzing power and the measured asymmetry in $\vec{p}p \to pp$ elastic scattering. As a result we obtain $P = (61.0 \pm 1.7)\,\%$. For that the pp analyzing power was taken from the SAID partial wave analysis [1]. The polar angular dependence is in good agreement with SAID and with a previous measurement by EDDA [9].

Possible systematic effects from different magnitudes of the + and - beam polarization were investigated by measuring both quantities independently. Within the experimental precision the two results, $P_+ = (66 \pm 4)\%$ and $P_- = (57 \pm 4)\%$, are compatible. An analysis of A_N using $P_\pm$ separately for the corresponding data samples yields a systematic deviation to the analyis with Eq. (11) of less than 30% of the statistical precision. Therefore, the difference is neglected in the following analysis.

4 Results

4.1 Dalitz Plot

The Dalitz plot of the selected event sample is shown in Fig. 3. It is corrected for the detector acceptance with MC generated events. The complete kinematic acceptance of the COSY-TOF detector is evident. The Dalitz plot density is strongly enhanced at $m^2_{p\Lambda} = 4.53\,\mathrm{GeV}^2/c^4$, i.e. the $N\Sigma$ threshold. This has been observed before [10, 11] and is usually interpreted as an $N\Sigma$–$p\Lambda$ coupled channel effect. The high resolution available in this measurement makes an analysis of the shape, position and strength of this structure interesting; however that is beyond the scope of this report. It is analyzed in more detail in Refs. [12, 13].

The enhancement of the production cross section close to threshold from $p\Lambda$ interactions, as discussed in Sec. 2, is clearly visible at low $m_{p\Lambda}$ values. The increasing differential cross section for decreasing $m_{K\Lambda}$ (see Fig. 3) can be explained by the influence of the resonances $N(1710)$ and/or $N(1720)$ [3, 4]. In the Dalitz plot these are located around $m^2_{K\Lambda} \approx 2.93\,\mathrm{GeV}^2/c^4$. However, due to their width of more than $100\,\mathrm{MeV}/c^2$ they do not appear as narrow structures. For a theoretical description see, e.g., Refs. [14, 15].

4.2 Effective Scattering Length

In Fig. 4 the $p\Lambda$ invariant mass spectrum is shown. Since the time integrated luminosity of the event sample is not needed for this analysis, only the number of measured events (N) scaled with the detector acceptance times reconstruction efficiency (A) is given. The quantity A has been determined with Monte Carlo studies and is included at the bottom of the figure. It is noteworthy, that the detector acceptance is nearly constant over a wide $m_{p\Lambda}$ range but varies between 27 % and 10% close to threshold.

For comparison, an arbitrarily scaled three-body S-wave phase-space distribution is shown with a solid line.

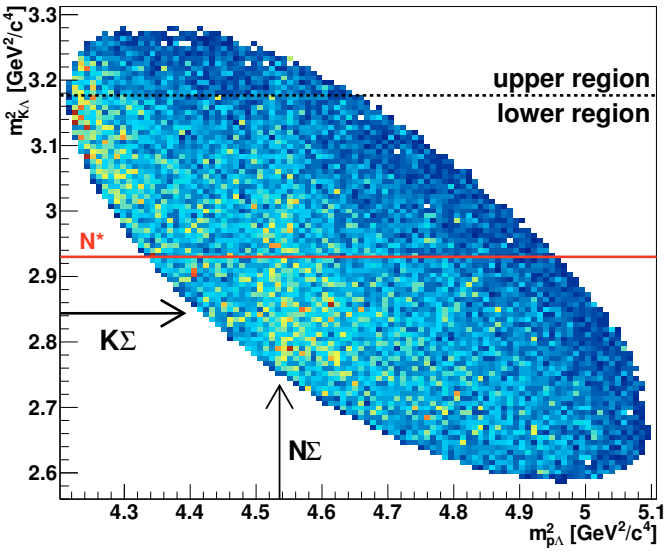

Fig. 3. The Dalitz plot of the reaction. Lighter colors indicate higher yield densities. The thresholds of the $N\Sigma$ and $K\Sigma$ channels are indicated by arrows, respectively. The region of the $N(1710)$ and $N(1720)$ resonances is indicated by a solid line. The dashed line marks the partition of the spectrum applied for the analysis discussed in Sec. 4.2

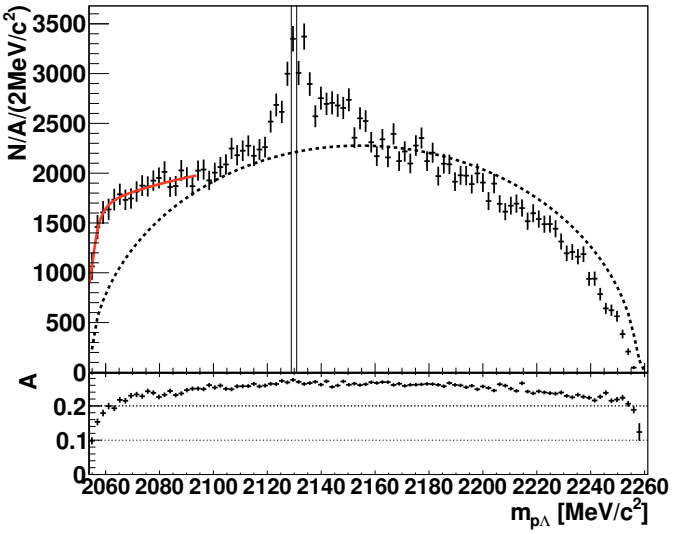

Fig. 4. The spectrum of $m_{p\Lambda}$ corrected for acceptance (A) as it is given on the bottom. The two vertical lines indicate the $N\Sigma$ thresholds. An arbitrarily scaled phase space distribution (dashed line) is shown to guide the eye. The solid line is a fit to the data as described in the text.

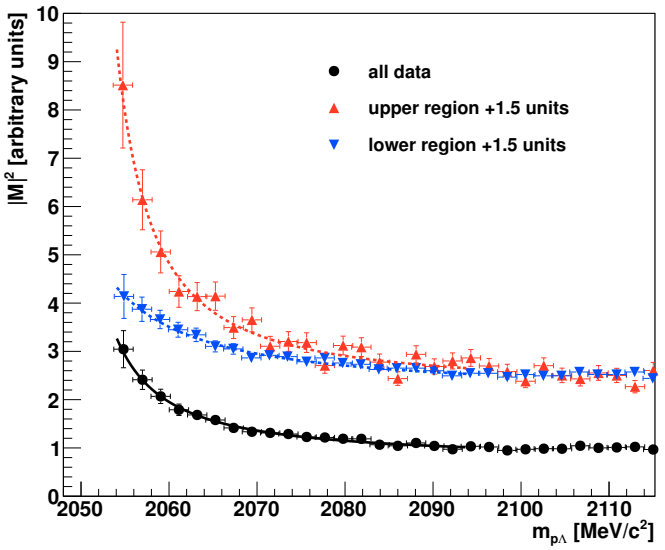

Fig. 5. The quantity $|M|^2$ (circles) fit with the exponential function of Eq. (3) (solid line). Results based on data from the upper (triangles up) and lower $m_{K\Lambda}$ region (triangles down) of the Dalitz plot alone, as described in the text, are also shown. For better readability the latter two are shifted +1.5 units on the y-axis, respectively.

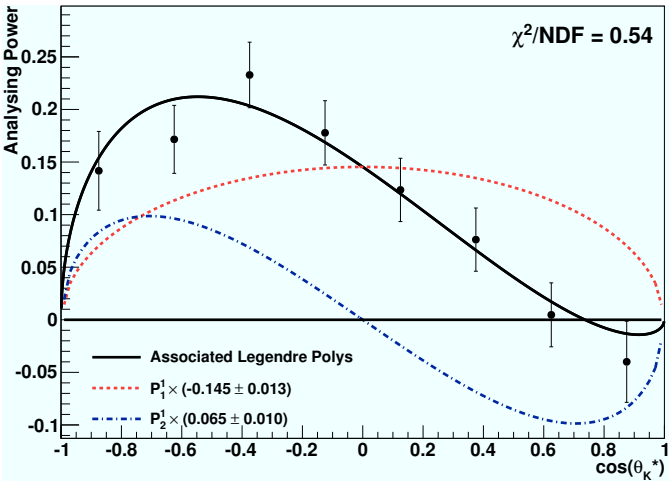

Fig. 6. The K^+ analyzing power for the whole $m_{p\Lambda}$ range. The fit (solid line) includes the associated Legendre polynomials (P_1^1) (dotted line) and (P_2^1) (dash-dotted line).

The $N\Sigma$ threshold positions of $m_{n\Sigma^+} = 2128.9\,\mathrm{MeV}/c^2$ and $m_{p\Sigma^0} = 2130.9\,\mathrm{MeV}/c^2$ are marked with two vertical lines. In this region a strong enhancement is visible.

There is also a sizable enhancement of the invariant mass spectrum at $m_{p\Lambda}$ values close to the $p\Lambda$ threshold, i.e. in the region relevant for the determination of the $p\Lambda$ scattering length. To test the method for the extraction of the scattering length the measured invariant mass spectrum is fit with the function given in Eq. (3), convoluted with the detector resolution. Within the range of $m_p + m_\Lambda \leq m_{p\Lambda} \leq m_p + m_\Lambda + 50$ MeV/c^2 the achieved χ^2/NDF is 0.32. The corresponding result is indicated by the solid line in Fig. 4.

From a likelihood analysis [2,7] of the highly correlated parameters we obtain $a_{\mathrm{eff}} = (-1.25 \pm 0.08 \pm 0.3)$ fm. Here, in the second and third term the uncertainties from statistics and of the theoretical method are given, respectively. Because the incoherent sum of the spin-singlet and spin triplet $p\Lambda$ final-state interactions enter into the production amplitude and their relative weights are unknown, a_{eff} is referred to as effective scattering length. Note, that it is not a spin average.

A variation of the upper limit of the fit range between (40, 50) MeV/c^2 yields a stable result within the statistical error. At an upper limit of 60 MeV/c^2 the absolute value of the effective scattering length increases by ≈ 0.3 fm. Although this is still within the systematic error, it might be connected to an increasing importance of higher partial waves in the $\{p\Lambda\}$ system or it could signal already the onset of distortions caused by the nearby $N\Sigma$ threshold.

As emphasized in Ref. [2], the error due to the possible excitation of resonances or, more generally, of a final-state interaction in the $K\Lambda$ and/or KN subsystems cannot be estimated on general grounds and, therefore, is not included in the theoretical uncertainty of 0.3 fm cited above. It can only be quantified via a careful analysis of the Dalitz plot.

For this purpose Fig. 5 presents the ratio of the spectrum to the arbitrarily scaled phase space (circles), see Eq. (7). Our fit based on the exponential function of Eq. (3) is shown by the solid line. The data are normalized to have an average $|M(m_{p\Lambda})|^2 = 1$ in the range $(2090 < m_{p\Lambda} < 2110)\,\mathrm{MeV}/c^2$. To quantify the influence of the N^* resonances on the measurement, we apply the method described above to two separate $m_{K\Lambda}$-regions of the Dalitz plot, namely $(2.590 \leq m^2_{K\Lambda} \leq 3.176)\,\mathrm{GeV}^2/c^4$ (triangles down) and $(3.176 \leq m^2_{K\Lambda} \leq 3.287)\,\mathrm{GeV}^2/c^4$ (triangles up). These two regions are referred to as the lower (ℓr) and upper (ur) ranges, respectively. Their boundaries are chosen such that both regions include $m_{p\Lambda} = m_p + m_\Lambda$, i.e. the near-threshold region relevant for the determination of the $p\Lambda$ scattering length. To improve readability the data are shifted by +1.5 units along the y-axis in Fig. 5.

It can be seen that the measured strength and shape of the final-state interaction varies significantly between all three samples. We obtain $a^{\ell r}_{\mathrm{eff}} = (-0.86 \pm 0.06 \pm 0.3)$ fm for the lower and $a^{ur}_{\mathrm{eff}} = (-2.06 \pm 0.16 \pm 0.3)$ fm for the upper range, respectively. The difference of 1.20 fm shows that the systematic effect of N^* resonances severely limits the precision of the determination of a_{eff} from our data. This result agrees with our observations for the Dalitz plot in Fig. 3: At low $m^2_{p\Lambda}$ the density clearly deviates from a homogeneous distribution along $m^2_{K\Lambda}$, leading to a tilted shape of the enhancement from final-state interactions.

4.3 K^+ Analyzing Power

In Fig. 6 the analyzing power of the K^+ is shown for the whole $m_{p\Lambda}$ range. The parameters $\bar{\alpha}$ and $\bar{\beta}$ of Eq. (5) are fit to the data (solid line). The good quality of the fit, χ^2/NDF $= 0.54$, justifies the exclusion of higher order contributions in Eqs. (1) and (5). The symmetric (dotted

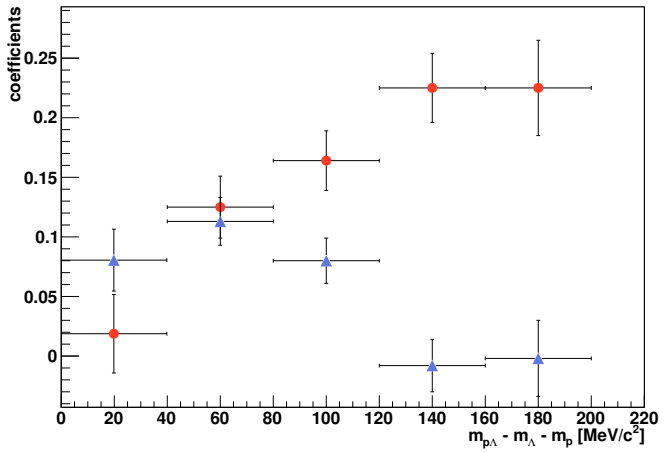

Fig. 7. The coefficients $\bar{\alpha}$ and $\bar{\beta}$ corresponding to the forward-backward symmetric (circles) and antisymmetric (triangles) contributions to the K^+ analyzing power as a function of $m_{p\Lambda}$ according to Eq. (5).

line) and antisymmetric contributions (dash-dotted line) are also shown separately.

In Fig. 7 the event sample is binned in $m_{p\Lambda}$ and the fit results for $-\bar{\alpha}(m_{p\Lambda})$ (circles) and $\bar{\beta}(m_{p\Lambda})$ (triangles) are given, respectively. The antisymmetric part of A_N approaches zero for higher $m_{p\Lambda}$. This is reasonable because in this region the K^+ has the lowest momentum which could be insufficient for s- and d-wave interference. The symmetric part on the other hand is close to 25% on the high end of the spectrum and reduces to $\leq 11\,\%$ with 3σ confidence on the low end. This means that with the present quantity of data the dependence of $\bar{\alpha}$ on $m_{p\Lambda}$ cannot be determined with sufficient precision to extract the spin-triplet scattering length with Eqs. (3-4).

5 Discussion

The observed behavior of the analyzing power is unexpected because in the reaction $pp \to d\pi^+$, that has only spin 1 in the final state and consequently the same selection rules, a value around 25 % for the symmetric contribution has been observed [16–18].

In principle, such small values could point to a complete absence of spin-triplet production in the reaction $pp \to pK^+\Lambda$. As discussed in Sec. 2, in that case contributions with even K^+ orbital angular momentum are zero at low $m_{p\Lambda}$. It would then follow that $a_{\rm eff}$ as determined in the last Section practically coincides with the $^1S_0$ scattering length a_s. However, one has to keep in mind that such small or vanishing contributions with even K^+ orbital angular momentum are only a necessary but not a sufficient condition for the absence of spin-triplet production, see Appendix B of [2]. Thus, based on the present experiment, the identification of our $a_{\rm eff}$ with a_s is purely hypothetical.

Realistic interaction potentials of the coupled $N\Lambda$–$N\Sigma$ systems [19–22] which describe $p\Lambda \to p\Lambda$ elastic scattering [23] and also the binding energy of the hypertriton [24, 25] predict $(-1.4 \leq a_t \leq -1.7)\,$fm and $(-2.5 \leq a_s \leq -2.9)\,$fm. Significantly smaller values of those scattering lengths, e.g. $a_s \approx -1.9$ fm as suggested by an investigation performed at leading order in chiral effective field theory [26] are no longer supported by the recent extension of this study to next-to-leading order [22]. Since the $N(1710)$ and $N(1720)$ resonances lie in the lower $m_{K\Lambda}$ region considered it is likely that their effect is weaker in the upper region. Therefore, if we interpret the extracted $a_{\rm eff}^{ur}$ as a lower boundary for the spin-singlet scattering length it would be still compatible with the theoretical picture, especially within the uncertainties. However, the value of $a_{\rm eff}^{ur}$ is more or less halfway between the ranges predicted for the singlet- and triplet $p\Lambda$ scattering lengths. This is also consistent with the naive expectation for this quantity if both spin states are produced.

Our $a_{\rm eff}^{ur}$ is in good agreement with the value published by the HIRES collaboration [27] which is $a = -2.4^{+0.16}_{-0.25}$. Their result is based on a combined analysis of FSI effects in the reaction $pp \to pK^+\Lambda$ at $p_{\rm beam} = 2.7\,$GeV/c and $p\Lambda$ elastic scattering data. If one takes into account the arguments of Ref. [28], where it is demonstrated that the method applied in Ref. [27] overestimates the scattering length by approximately 0.4 fm, the agreement is even better. Certainly, the effect of N^* resonances on the HIRES result is unclear, even though earlier measurements of COSY-TOF indicate a reduced influence on the Dalitz plot [3] at that beam momentum. Note that the authors of Ref. [27] argue that, based on their analysis, the production of the $p\Lambda$ system in a spin-triplet state is negligible.

As already said above, the behavior of the analyzing power as found in our experiment does not rule out the presence of spin-triplet $p\Lambda$ states: Since only the imaginary parts of the amplitudes enter the analyzing power, an accidental phase cancellation is possible. Definite conclusions can only be drawn if one can set quantitative upper limits for the symmetric part of the analyzing power. It is therefore important to collect higher statistics and measure at different beam energies. It should also be investigated how other polarization observables, e.g. the Λ polarization, can be employed to put quantitative constraints on the production of $p\Lambda$ in a spin-triplet state.

6 Conclusion

The effective $p\Lambda$ scattering length has been determined from final-state interactions in the reaction $\vec{p}p \to pK^+\Lambda$ at $p_{\rm beam} = 2.95\,$GeV/c. An examination of the influence of the excitation of N^* resonances in the $K\Lambda$ channel revealed that they introduce a large uncertainty on the analysis. This should be and has to be taken into account in any attempt to determine the $p\Lambda$ scattering length from this reaction. Whether the influence of those resonances is only particularly strong at beam momenta like those of the present experiment remains to be seen. For further studies, data from different beam momenta is highly desirable. Eventually, this could allow to quantify and even control the effect from resonances. It might even be possible to

identify a range of beam momenta where the presented method is not systematically distorted.

The K^+ analyzing power has been measured as a function of the $p\Lambda$ invariant mass. The vanishing symmetric contribution to the analyzing power at low values of $m_{p\Lambda}$ prohibits the extraction of the spin-triplet scattering length with the present quantity of data. The hypothesis of exclusive spin-singlet production of the $p\Lambda$ system was discussed as an explanation for this unexpected behavior. For a decisive study, measurements with higher statistics are needed. Especially, the possibilities to exploit the Λ polarization should be investigated.

7 Acknowledgments

The research leading to these results has received funding from the European Union Seventh Framework Programme (FP7/2007-2013) under grant agreement no. 283286.

This work comprises part of the PhD thesis of Matthias Röder.

We would like to thank the COSY operation crew for providing excellent quality beams.

References

1. R. A. Arndt, I. I. Strakovsky, and R. L. Workman, Phys. Rev. C **62**, 034005 (2000).
2. A. Gasparyan, J. Haidenbauer, C. Hanhart, and J. Speth, Phys. Rev. C **69**, 034006 (2004).
3. S. Abd El-Samad et al., Phys. Lett. B **688**, 142 (2010).
4. M. Abdel-Bary et al., Eur. Phys. J. A **46**, 27 (2010).
5. A. Sibirtsev, J. Haidenbauer, H.-W. Hammer, and S. Krewald, Eur. Phys. J. A **27**, 269 (2006).
6. C. Hanhart, Phys. Rept. **397**, 155 (2004).
7. M. Röder, *Final State Interactions and Polarization Variables in the Reaction $pp \to pK\Lambda$*, PhD thesis, Universität Bochum, 2011.
8. P. Wintz [COSY-TOF Collaboration], AIP Conf. Proc. **698**, 789 (2004).
9. M. Altmeier et al., Phys. Rev. Lett. **85**, 1819 (2000).
10. T. Tan, Phys. Rev. Lett. **23**, 395 (1969).
11. R. Siebert et al., Nucl. Phys. A **567**, 819 (1994).
12. H. Machner, J. Haidenbauer, F. Hinterberger, A. Magiera, J. A. Niskanen, J. Ritman, and R. Siudak, Nucl. Phys. A **901**, 65 (2013).
13. S. El-Samad et al., Eur. Phys. J. A **49**, 41 (2013).
14. J. -J. Xie, H. -X. Chen, and E. Oset, Phys. Rev. C **84**, 034004 (2011).
15. A. Gasparian, J. Haidenbauer, C. Hanhart, L. Kondratyuk, and J. Speth, Phys. Lett. B **480**, 273 (2000).
16. E. L. Mathie et al., Nucl. Phys. A **397**, 469 (1983).
17. D. A. Hutcheon, AIP Conf. Proc. **221**, 111 (1991).
18. E. J. Korkmaz et al., Nucl. Phys. A **535**, 637 (1991).
19. T. Rijken, V. Stoks, and Y. Yamamoto, Phys. Rev. C **59**, 21 (1999).
20. K. Tominaga and T. Ueda, Nucl. Phys. A **693**, 731 (2001).
21. J. Haidenbauer and U.-G. Meißner, Phys. Rev. C **72**, 044005 (2005).
22. J. Haidenbauer, S. Petschauer, N. Kaiser, U.-G. Meißner, A. Nogga, and W. Weise, Nucl. Phys. A **915**, 24 (2013).
23. G. Alexander et al., Phys. Rev. **173**, 1452 (1968).
24. A. Nogga, H. Kamada, and W. Glöckle, Phys. Rev. Lett. **88**, 172501 (2002).
25. A. Nogga, Nucl. Phys. A **914**, 140 (2013).
26. H. Polinder, J. Haidenbauer, and U.-G. Meißner, Nucl. Phys. A **779**, 244 (2006).
27. A. Budzanowski et al., Phys. Lett. B **687**, 31 (2010).
28. A. Gasparyan, J. Haidenbauer, and C. Hanhart, Phys. Rev. C **72**, 034006 (2005).